



CONTACTLESS POWER TRANSFER SYSTEM- HARDWARE ANALYSIS

Presentation By **Dr. Praveen Kumar**

Associate Professor

Department of Electronics & Communication Engineering



Overview

2

- Introduction
- Computation of mutual inductance for square coils
- Generalized computation of mutual inductance for coils of different geometries
- Ongoing and future works

Introduction

3

- It is important to analyze the contactless system by developing a hardware prototype to check its real time functioning.
- This presentation explains some hardware works in contactless system done at IITG and some glimpse of ongoing and future works.
- The prototype of contactless system mainly involves the following factors, to perform power conversion tasks required at different stages.
 - i. The development of converters and controllers.
 - ii. Design of compensation capacitors, filter capacitors and inductors.

Introduction (Contd.)

4

- In addition, the magnetic coupling of the coils mainly depends on mutual inductance (MI) between the coils.
- Therefore, computation of MI is one of the crucial factor in the design of contactless system and will play a key role in determination of efficiency and power transferred.

Mutual inductance (MI) between two square coil

Mutual inductance (MI) between two square coil

6

- The analysis presented in this paper computes MI between two air core square coils, placed in a flat planar surface coinciding in space.
- The air core square coil has mutually coupled primary and secondary coil.
- The coil which is excited is referred as excitation coil (EC) and the coil where the output variations are observed is referred as observation coil (OC) as shown in Fig.1.

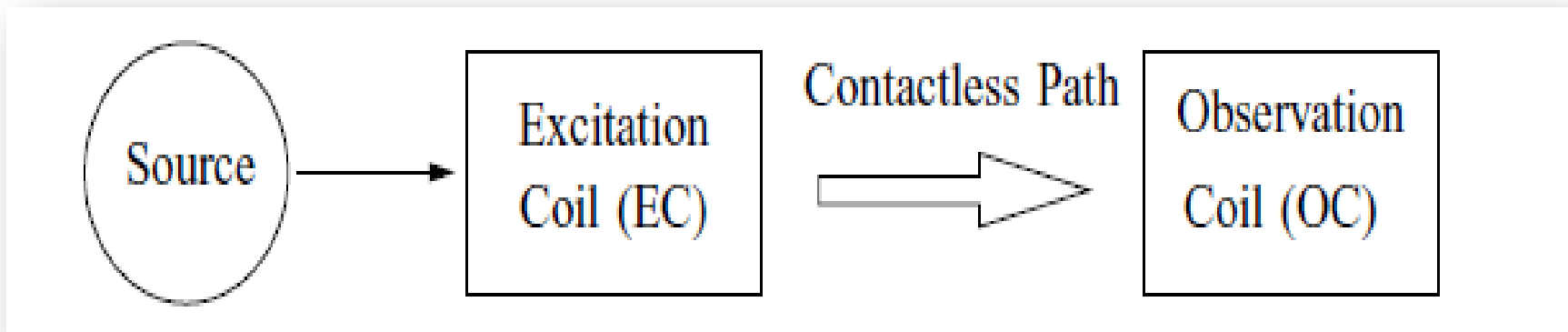


Fig.1. Block diagram of contactless system

Mutual inductance (MI) between two square coil (Contd.)



7

- As the MI of the coil varies with the change in position of the coils, different variations of the coils i.e. Misalignments are analyzed.
- Different cases of variations of OC with respect to EC are taken into account, which are shown in Fig. 2.

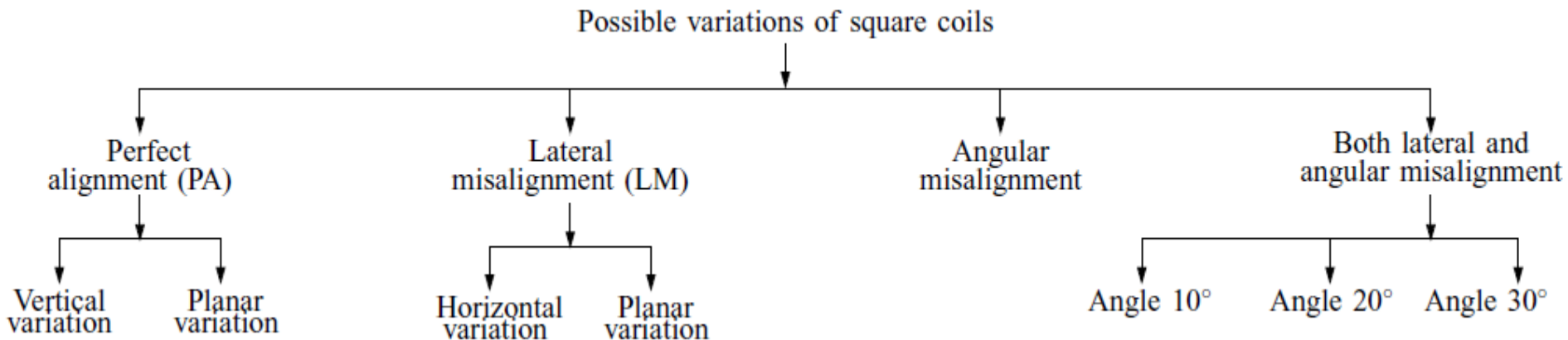


Fig.2. Possible variations of contactless coil

Mutual inductance (MI) between two square coil (Contd.)



8

- The schematics of different variations of coil is shown in Fig.3

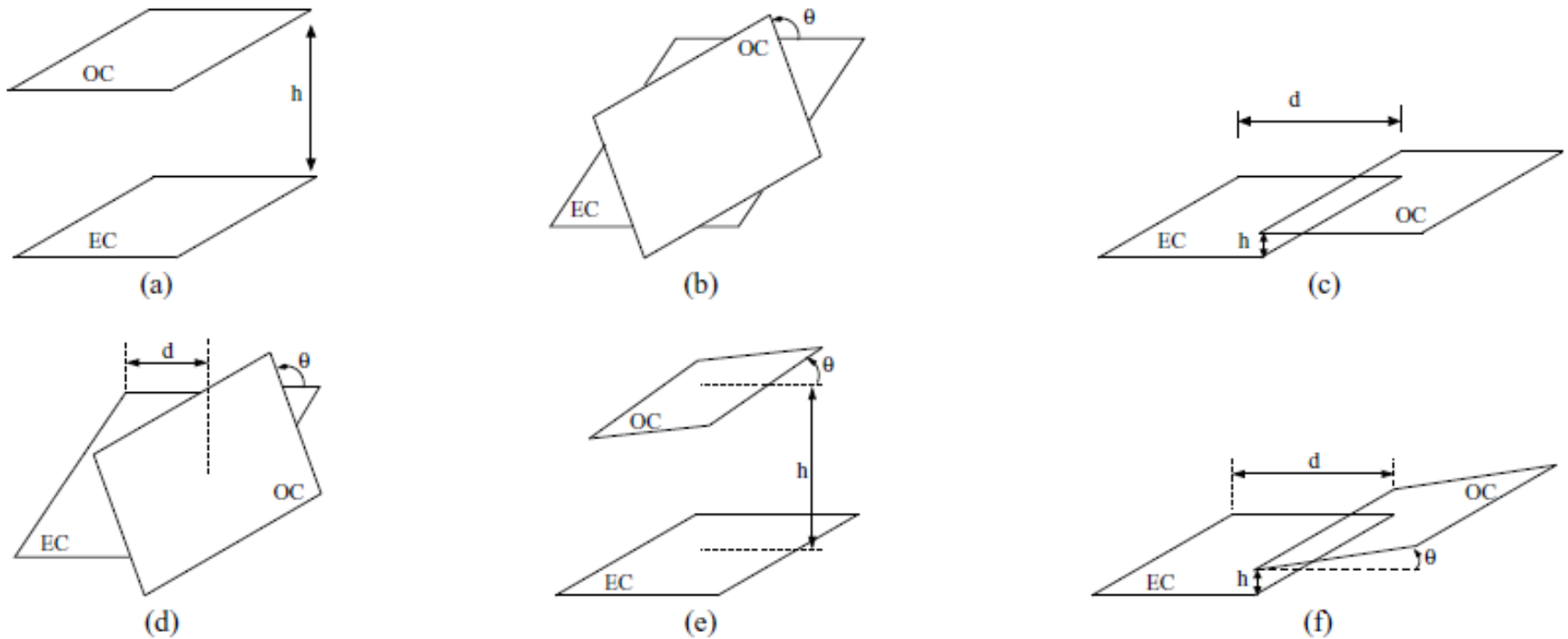


Fig.3. Schematics of square coils for analyzed variations (a) PA - Vertical variation (b) PA - Planar variation (c) LM - Horizontal variation (d) LM - Planar variation (e) Angular misalignment (f) Both lateral and angular misalignment.

Terminologies used to refer variation of square coil



9

- **Perfect alignment:** If EC and OC are placed in a flat planar surface with coinciding axes, such arrangement of coils is referred as *perfect alignment (PA)*.
- **Lateral misalignment:** If coils are situated in parallel plane and displaced horizontally, such arrangement of coils is referred as *Lateral misalignment (LM)*.
- **Angular misalignment:** If OC is titled up or down with certain angle ($<90^\circ$) due to unequal surface impacts; such arrangement of coils is referred as *angular misalignment*.
- **Both lateral and angular misalignment:** If OC is both tilted and varied horizontally, such arrangement of coils is referred as *both lateral and angular misalignments*.

Mutual inductance (MI) between two square coil (Contd.)



10

- The coil parameters used in Fig.3 is described in Table I.

Parameter	Description
EC, OC	Excitation coil, observation coil
h	Deviated vertically from the center of the coil
d	Deviated horizontally from the center of the coil
θ	Angle of OC with respect to EC

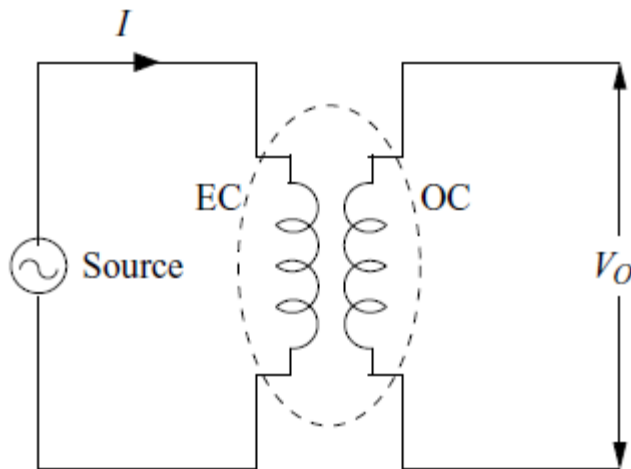
Table I: Coil Parameters

Analytical modeling of square coil



11

- The circuit topology of the inductive coils resembles an inductively coupled transformer, represented by an equivalent circuit shown in Fig. 4.



- I - supply current
- λ_1 - magnetic flux
- λ_{12} - mutual flux
- EC - Excitation coil
- OC - Observation coil
- V_o - Voltage across the secondary coil

Fig.4. Equivalent circuit model of an inductive coil

Analytical modeling of square coil (contd.)



12

- MI between two coupled coils can be calculated from the basic expression as given by (1)

$$M = \frac{\lambda_{12}}{I_1} \quad (1)$$

- The flux linked with the OC (λ_{12}) due to current in the EC can be calculated analytically by considering the flux distribution of each individual coil turns of the OC.
- The area enclosed by the selected turn of OC is divided into small regions and thereby considering the complete spiral square coil.
- The flux through each small region of the OC is taken into account to calculate the flux linked to OC due to EC.

Analytical modeling of square coil (contd.)



13

- A sequence of program routine have been used to carry out this process
- The total flux linked in the OC is obtained by the sum of the flux linked in each small grid for all the turns of the OC.
- Assuming φ_n is the flux linked with the n^{th} region of the area enclosed by single turn of the OC, then λ_{12} can be estimated by (2).

$$\lambda_{12} = \sum \varphi_n \quad (2)$$

- The limit of the summation depends on the number of small regions formed in a single turn of OC.

Analytical modeling of square coil (contd.)



14

- The flux linked to each of these small regions of OC due to EC is calculated with the following assumptions.
 - i. The insulated coil conductors are placed such that there is no space between conductors of any two loop and they are touching each other.
 - ii. The magnetic field in the small region of the coil (Fig. 5) is assumed to be constant and its value is calculated at the center of the

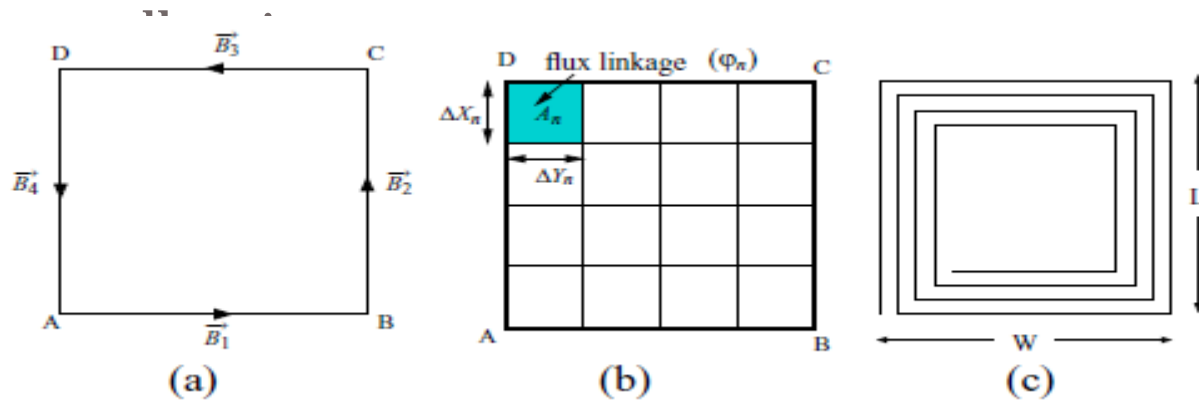


Fig. 5. Square current carrying coil (a) Single turn (b) Single turn segmented (c) Multiple turn.

Analytical modeling of square coil (contd.)



15

- Based on these assumptions, ϕ_n for each small region is calculated using (3) and (4), which depends on the magnetic field at the center of the small region, n^{th} area (A_n) and normal vector of the n^{th} area (\vec{B}_c)

$$A_n = \Delta x_n \cdot \Delta y_n \quad (3)$$

$$(\hat{A}_n)$$

$$\phi_n = \vec{B}_c \cdot (A_n \cdot \hat{A}_n) \quad (4)$$

- Where, Δx_n and Δy_n are the length and width of the small divided region as shown in Fig. 5(b).
- The magnetic field (\vec{B}_c) at the center of the small region is caused due to EC.
- (\vec{B}_c) is calculated for P turns of EC and is given by (5).

$$\vec{B}_c = \sum_{m=1}^P \vec{B} \quad (5)$$

Analytical modeling of square coil (contd.)



16

- The individual coil turns of EC is modeled by four straight current carrying conductors.
- Let (\vec{B}) is the magnetic field due to one current carrying loop of EC as shown in Fig. 5(a) and is given by (6).

$$B = \sum_{n=1}^4 \vec{B}_n \quad (6)$$

- In the above equation, n represents the four sides of the single current carrying loop.
- The (\vec{B}_1) , (\vec{B}_2) , (\vec{B}_3) and (\vec{B}_4) are the magnetic fields of the sides of the square coil AB, BC, CD and DA.
- (\vec{B}_n) can be calculated from the Bio-Savart law for magnetic field.

Analytical modeling of square coil (contd.,)



17

- The basic magnetic field equation (\vec{B}_n) at any point in space due to a straight current carrying conductor is given by (7).

$$\vec{B} = \int \frac{\mu_0 I \vec{ds} \times \hat{R}}{4\pi R^2} \quad (7)$$

- Where, \hat{R} is the unit vector in the direction of position vector of the observation point, originating from the differential element of current carrying conductor (\vec{ds})
- The direction of \vec{ds} is in the direction of current in the conductor. The integration in (6) is performed over the length of the conductor.
- Similarly, the magnetic field at a point in space and flux linkage calculations can be done for spiral square coils with multiple turns as shown in Fig. 5(c), where L and W are the length and width of the coil.

Numerical Evaluation

18

- The procedure for numerical calculation is explained in the following steps.
 - i. The total number of turns for EC (P) and OC (Q) are determined.
 - ii. 3D co-ordinates of a single turn of EC and OC are determined.
 - iii. Diameter of conductor and distance between EC and OC (depending on the type of variation) is determined.
 - iv. The selected turn of the coil is divided into multiple small areas from A_1, \dots, A_n as shown in Fig. 5(b).
 - v. Calculate the total flux linked to each small area of OC using (8) by calculating the magnetic field at the center .

$$\varphi_1 = \sum_{n=1}^4 \frac{\mu_o}{4\pi} \int \frac{I \vec{ds} \times \vec{R}}{R^2} \cdot (\vec{A} \cdot \vec{A}) \quad (8)$$

Numerical Evaluation

19

- The flux linked in a single turn (φ_m) of OC is obtained by summing all the fluxes using (9).

$$\varphi_1 = \sum_{k=1}^p \sum (\varphi_1 + \varphi_2 + \dots + \varphi_n) \quad (9)$$

- This procedure is repeated for all turns of EC and OC and λ_{12} is calculated using (10).

$$\lambda_{12} = \sum_{m=1}^q \varphi_m \quad (10)$$

- Therefore from these equations MI is calculated using (1).
- This procedure has been used for all variations of EC and OC with their corresponding new coordinates and vertices.



Numerical Evaluation (contd)

20

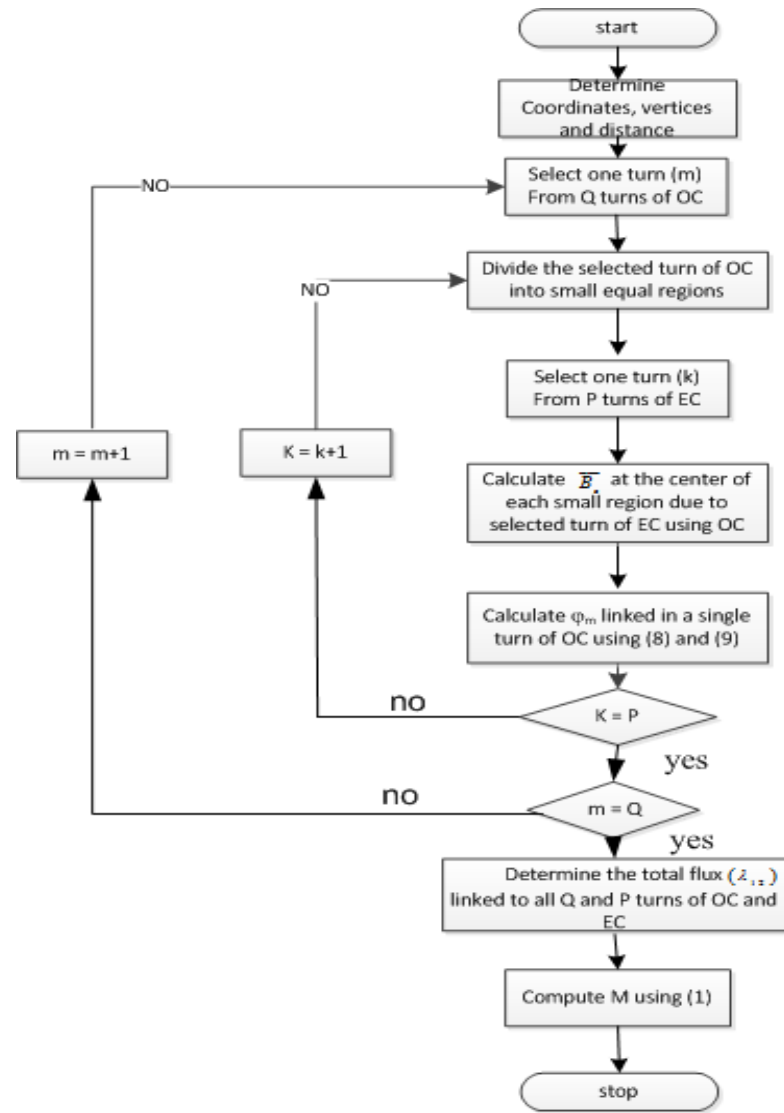
- Thus, the method adapted in this work has used only Biot - Savart law for a straight current carrying conductor; which is the basic equation for calculating the magnetic field.

Flow chart describing numerical evaluation



21

Fig. 6. Flow chart describing numerical evaluation.



Finite element modeling

22

- The commercial 3-D finite element tool ANSYS Maxwell 14.0.0 has been used for validating the analytical model.
- The EC and OC considered in this work have 11 and 9 turns respectively.
- The EC is excited with a current of 10A.
- The EC and OC are modeled for different variations and are analyzed by changing their co-ordinates in simulation environment.
- The models are created using the co-ordinates taken from the experimental setup.
- The FEA models are formed for all the configurations of the coils and various positions of OC by changing its coordinates.



Finite element modeling (contd.)

23

- To simplify the analytical calculations and to reduce the computation time, following assumptions are made in this investigation for flux linkage calculations.
 - i. As the 3-D FEA model for spiral square coil takes very long time and sophisticated computation environment, the models are analyzed with all the dimensions reduced to one fifth of the original. This adjustment is justified as the variation of the flux linkage is linear with the dimension of the whole system, which can be proved analytically.
 - ii. To reduce the computational time, OC is put as a surface whose area is equal to that of EC and flux linked to the surface has been calculated.
 - iii. The multiple turns of EC and OC are assumed to be placed near with no space between the turns of the coils.

Finite element modeling (contd.)

24

- Fig. 7 shows the FEA models of the coils for different variations such as vertical, angular and planar.
- The flux linked in the OC due to EC is found by integrating the magnetic field over the area of OC using Maxwells field calculator.

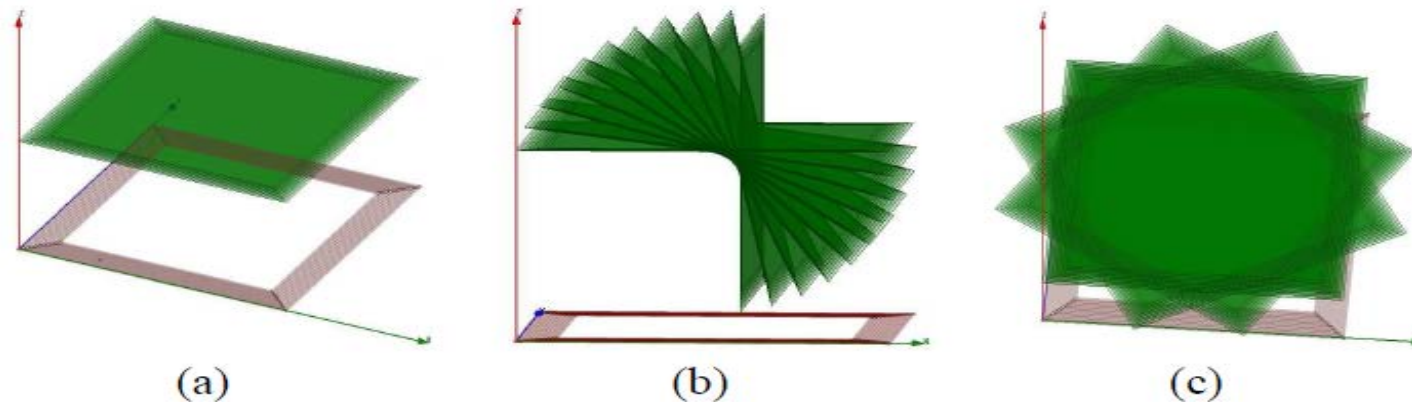


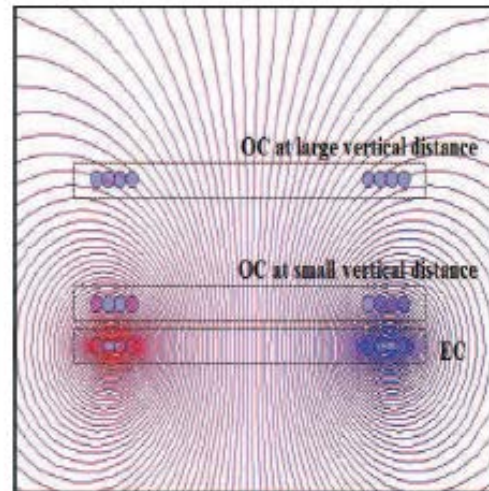
Fig.7. FEA models of square coils for different variations (a) Vertical (b) Angular (c) Planar.

Finite element modeling (contd.)

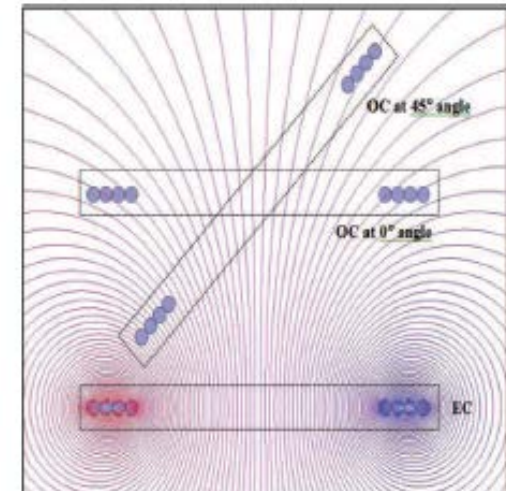
25

- Fig. 8 shows the 2D plot of magnetic field lines of EC and OC having four conductors each.
- Fig. 8(a) shows two positions of vertical variation of OC at small and large distances. Fig. 8(b) shows two positions of angular variation of OC at 0° and 45° angles.

Fig. 8. Magnetic field lines for cut section of coils (a) Vertical (b) Angular



(a)



(b)

Experimental verification

26

- In order to verify the analytical and FEA results an experimental setup is built in the laboratory.
- Table II shows the specifications of the components used for evaluation.

TABLE II
SPECIFICATIONS OF THE COMPONENTS

Parameter	Description	Value
V_{dc}	DC supply	0-30V
L_p	Inductance of EC	$54\mu\text{H}$
L_s	Inductance of OC	$37\mu\text{H}$
f	Frequency	18kHz
C_f	Filter capacitor	$1.44\mu\text{F}$
W	Width of the coil	18cm
L	Length of the coil	18cm
N_p	Number of turns in EC	11
N_s	Number of turns in OC	9

Experimental verification (contd.)



27

- The circuit topology and its control blocks are shown in Fig. 9 and Fig. 10.
- The filter capacitor has been calculated using the formula given by (11).

$$C_f = \frac{1}{\omega^2 L_p} \quad (11)$$

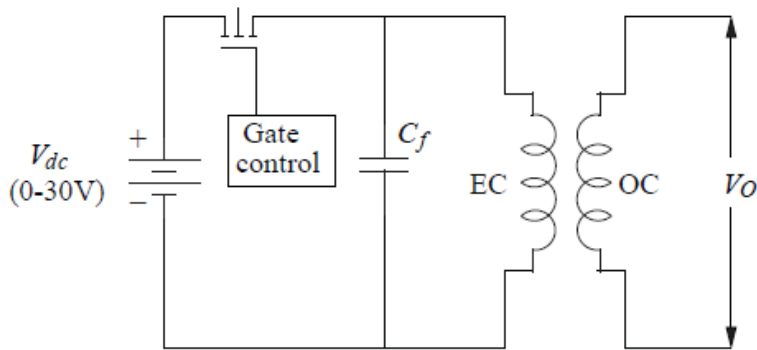


Fig.9. Schematic representation of power circuit.

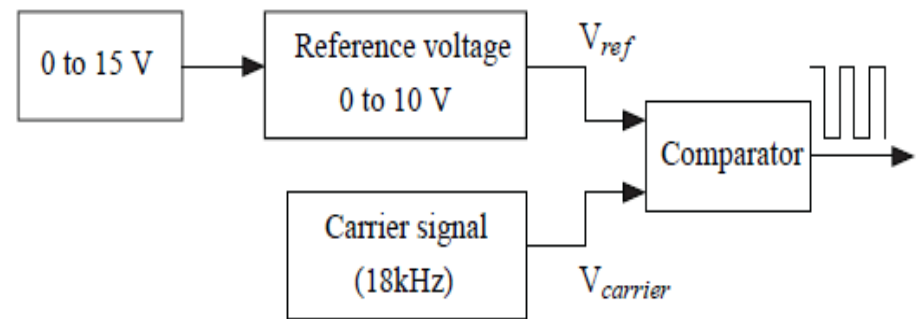


Fig. 10. Controller blocks.

Experimental verification (contd.)



28

- The details of experimental setup for different variations are briefly explained below:
 - i. For vertical variation, the arrangement in wooden staff is made to vary the distance between OC and EC.
 - ii. For planar variation, the whole supporting system of wooden staff is rotated in a circle around EC.
 - iii. For lateral variation, the wooden staff arrangement is made such that OC can be moved over the wooden staffs horizontally.
 - iv. For angular misalignment, OC is fixed in a supporting rod above EC at a vertical height and tilted.

Experimental verification (contd.)



29

- Fig. 11 shows the complete hardware arrangement made for the experimental evaluation of MI.
- The schematics of different variations are shown in Fig. 12.

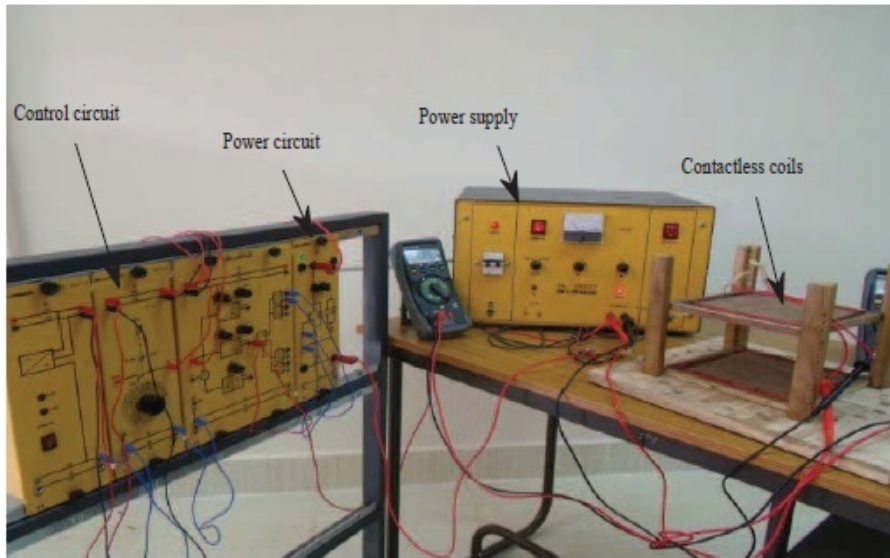


Fig.11. Experimental setup for mutual inductance computation

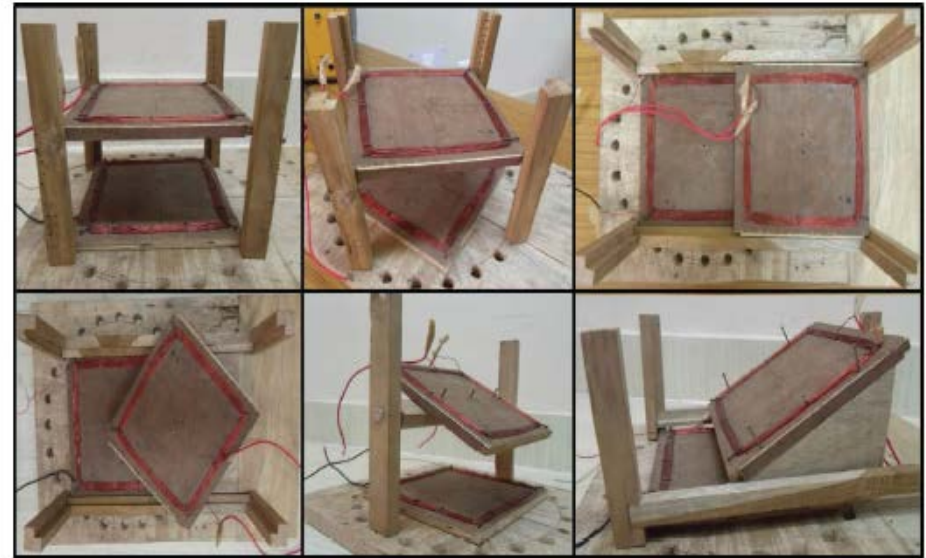


Fig. 12. Possible variations of coils

Experimental verification (contd.)



30

- The conductors of the coils are placed such that there is no space between the conductors of any two loop and they are not touching each other.
- The conductors are spread in a distance of 1.98cm and 1.65cm for EC and OC. The inner area which is not occupied by the conductor is 197.12cm² and 216.27cm² for EC and OC respectively.
- The experimental setup built is made to analyze all possible position of the coil including lateral and angular misalignments.
- The formula used for experimental computation of MI is given by

$$MI = \frac{V_{OC}}{V_{EC}} L_p \quad (12)$$

Numerical results and discussion

31

- The numerical results obtained from three analysis such as analytical method, finite element model and an experimental setup has been analyzed and compared.
- In order to compare the results, this study has considered the following general points:
 - i. Maximum and minimum variations of vertical distance between EC and OC have been taken as 10cm and 2 cm.
 - ii. Maximum and minimum variation in horizontal direction have been taken as 11.4cm and 0cm.
 - iii. The maximum rotational variation considered is 90° . This is because the MI value would be repetitive for square geometry for angle beyond 90° .
 - iv. The vertical and horizontal distances are increased by 1cm for subsequent observations.
 - v. The planar variation is recorded for a sequence of angles at an interval of 10° while, due to practical constraints the experimental readings are recorded for a step of 15° change.

Numerical results and discussion (contd.)



32

Perfect Alignment - Vertical and Planar Variation

- Fig. 13 and Fig. 14 shows the graphical plots of perfectly aligned curve with vertical and planar variation

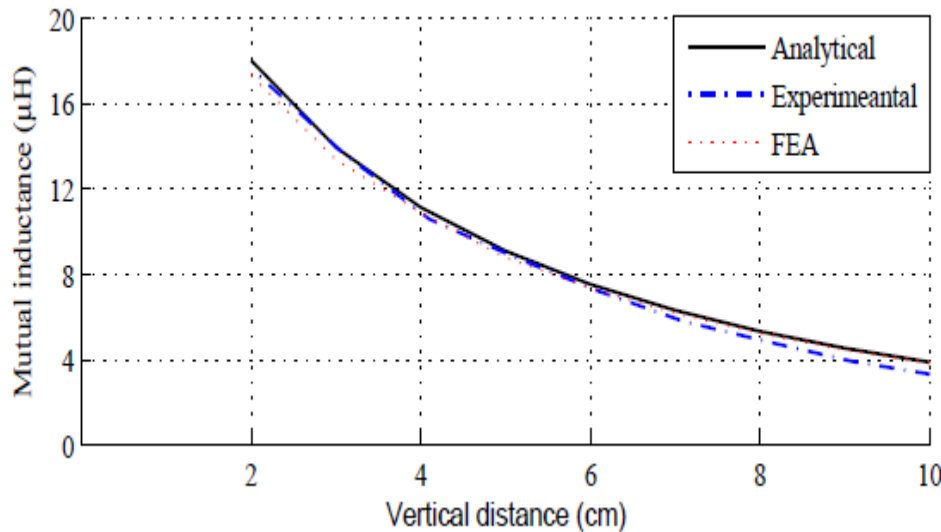


Fig. 13. Perfect alignment - vertical variation.

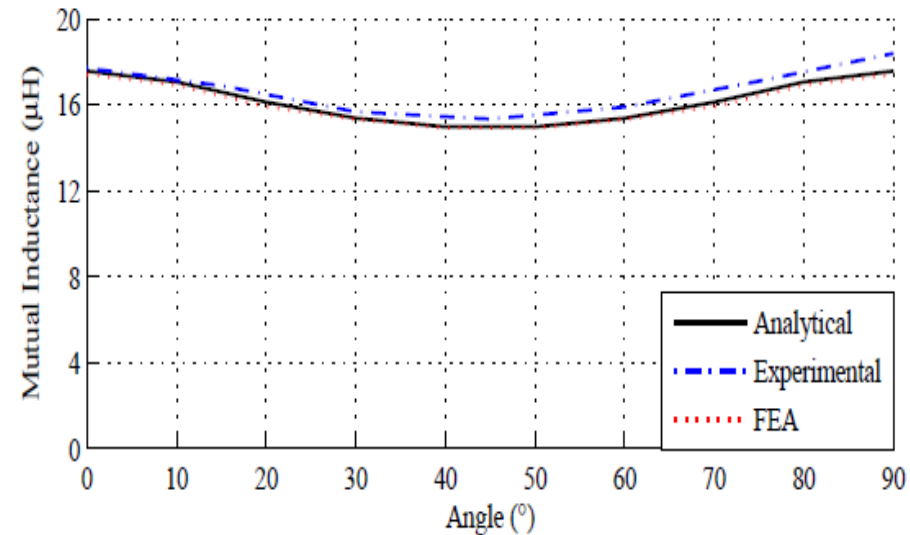


Fig. 14. Perfect alignment - planar variation.

Numerical results and discussion (contd.)



33

Lateral Misalignment - Horizontal and Planar Variation

□ Fig. 15 and Fig. 16 shows the graphical plots of Lateral Misalignment with horizontal and planar variation

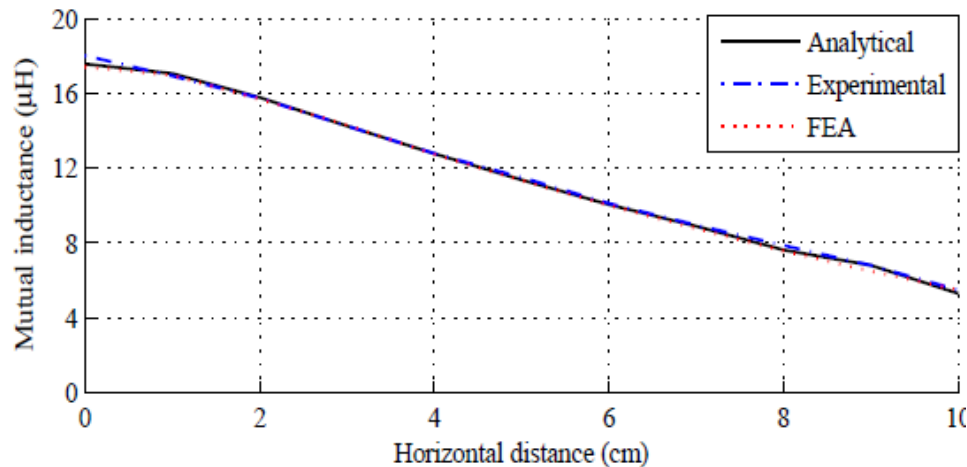


Fig. 15. Lateral misalignment - Horizontal variation..

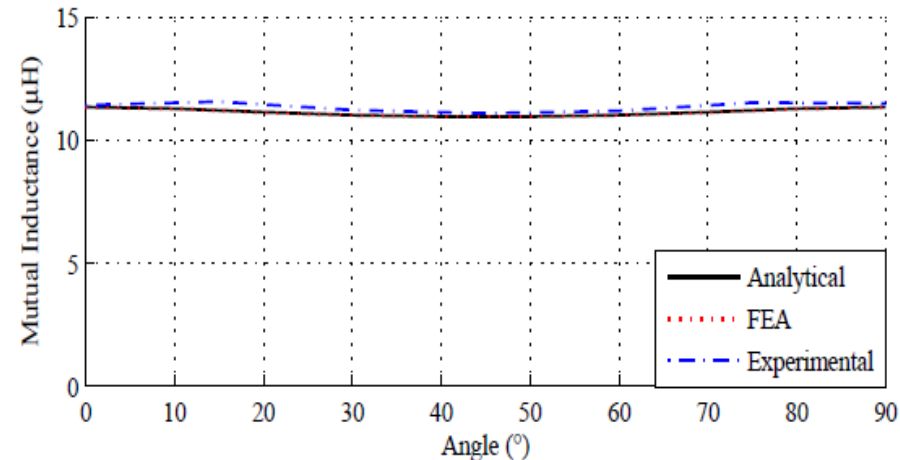


Fig. 16. Lateral misalignment - Planar variation.

Numerical results and discussion (contd.)



34

Angular Misalignment, Both Lateral and Angular Misalignment

□ Fig. 17 and Fig. 18 shows the graphical plots of angular misalignment and both lateral and angular misalignment.

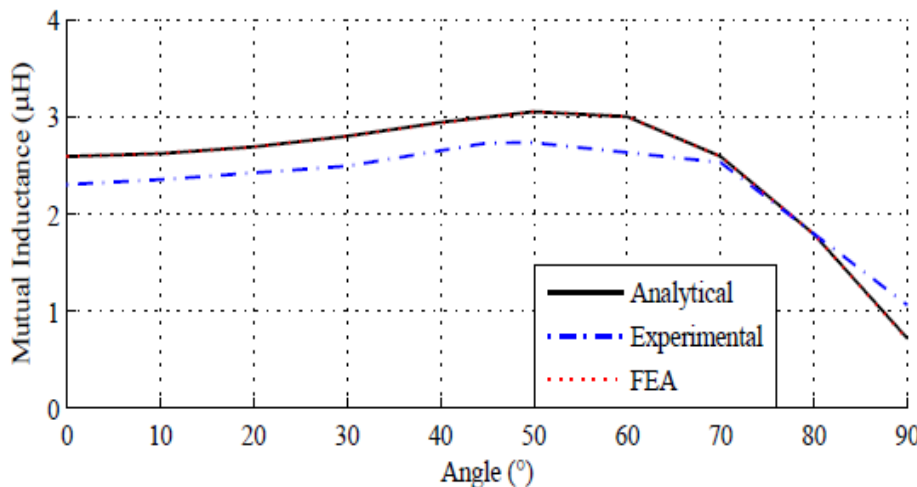


Fig. 17. Angular misalignment - angular variation

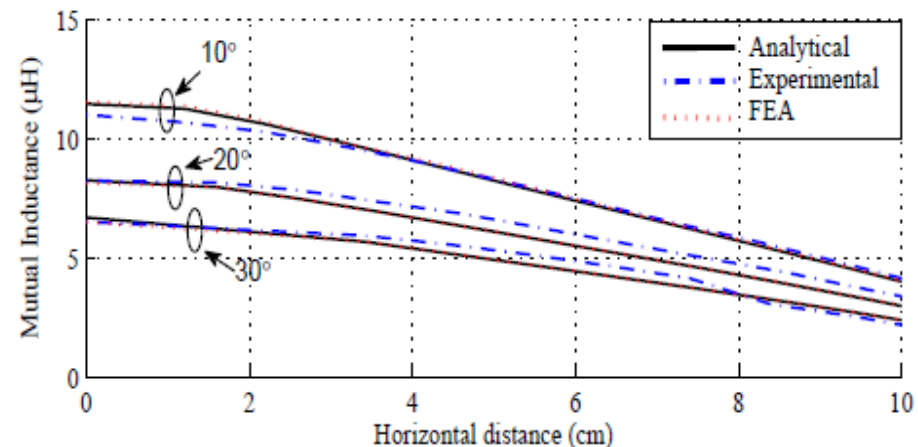


Fig. 18. Both lateral and angular misalignment (Angle=10°, 20°, 30°).

Illustration of calculation Procedure



35

- Consider two square coils of length and width of 18cm having a conductor diameter of 1.83mm.
 - The number of turns for excitation (EC) and observation coils (OC) are 11 and 9. The current flow in EC is taken to be 10A.
 - The following cases of variations are chosen for explanation of analytical model.
 - *Case I: Perfect alignment - vertical variation: OC kept at a vertical height of 2cm with respect to EC.*
 - *Case II: Perfect alignment - planar variation: OC kept at vertical height of 2.1cm and rotated with an angle of 10°.*
 - *Case II: Perfect alignment - planar variation: OC kept at vertical height of 2.1cm and rotated with an angle of 10°.*

Mutual inductance (MI) between two square coil (Contd.)

- The numerical values obtained in each step for multiple turns of OC are summarized in Table VIII for the above considered cases.
- The flux linkage for each turn of OC is calculated using (8) and (9).
- From these results, the total flux linkage and mutual inductance is calculated using (10) and (1).

	Case I	Case II	Case III	Case I	Case II	Case III
	(μWb)					
ϕ_1	20.78	19.72	3.27	ϕ_6	20.03	18.87
ϕ_2	20.81	19.69	3.18	ϕ_7	19.60	18.49
ϕ_3	20.76	19.59	3.10	ϕ_8	19.09	18.04
ϕ_4	20.61	19.42	3.01	ϕ_9	18.49	17.52
ϕ_5	20.37	19.18	2.92			
λ_{12}	180.50	170.50	26.20			
M	$18.05\mu\text{H}$	$17.05\mu\text{H}$	$2.62\mu\text{H}$			

Table III
Results of sample calculation

Conclusions

37

- The following conclusions are drawn from the work:
 - i. When the coils are placed close to each other with coinciding axes, MI values are maximum; which indicates high coupling between the coils and expected to have maximum power transfer in contactless systems.
 - ii. At large coil distances, relatively large horizontal and vertical misalignments; MI have no significant effects. This indicates relatively low coupling and it would not transfer any power.
 - iii. In planar variation, MI value would vary marginally. Such type of variation would not affect the power transfer in contactless systems.
 - iv. In angular misalignment, tilting OC at certain angle brings half of the coil closer to the perimeter of EC and due to this MI value increases and for other angles, MI values would suddenly decrease. Such type of variations in practical systems would cause instability.

Mutual inductance for coils of different geometries

Semi analytic computation method



39

- In this work, generalized semi analytic computation method for MI has been explained for different coil geometries.
- Coil geometries such as rectangle, circle, ellipse, hexagon and pentagon have been used.
- The coil geometries analyzed in this work is depicted in Fig. 19.

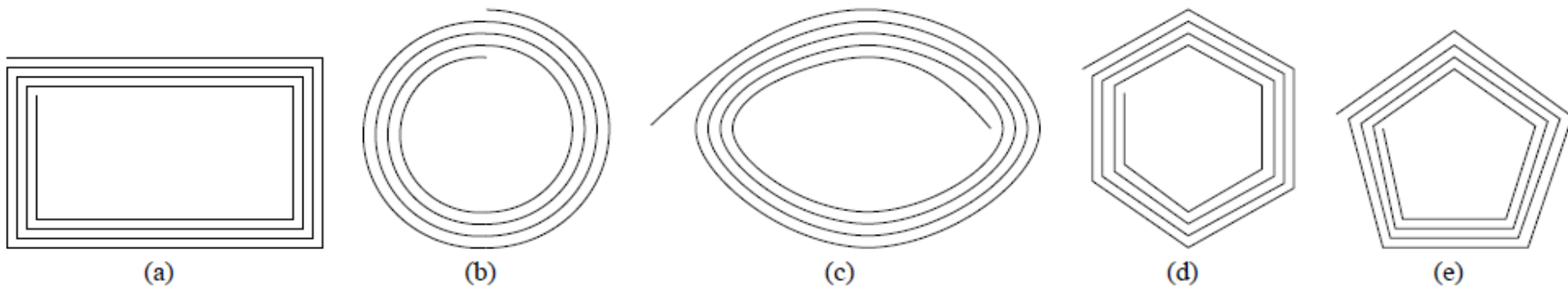


Fig. 19. Schematics of spiral arrangement of different coil geometries (a) rectangular (b) circular (c) elliptical (d) hexagonal (e) pentagonal.

Semi analytic computation method (contd.)



40

- The MI of two coupled coils can be calculated from the basic expression as given by (1).
- Here, the technique used for calculating λ_{12} for different coil geometries is different from the former computation.
- λ_{12} linked to the SC due to PC is calculated semi analytically based on the discretization of individual coil turns of SC due to PC.
- A computer program routine used which automatically divides the interior of the coil geometries into *triangular elements* with specifications of the basic parameter defining the geometry of the coil.

Semi analytic computation method (contd.)



41

- The flux (ϕ_i) crossing through the i^{th} triangular element is given by (13).

$$\phi_i = (\vec{B}_{cent})_i \cdot (A_i \cdot \vec{A}_i) \quad (13)$$

Where, i varies from 1 to Q , Q is the number of discretized triangular element present in the single turn of the coil. A_i is the area of the i^{th} triangular element. \vec{A}_i is the normal vector perpendicular to the plane of the i^{th} area.

$(\vec{B}_{cent})_i$ and \vec{A}_i are calculated from the coordinates of the vertices of the triangular element obtained from automatic mesh generation.

- A_i is the magnetic field at the center of the i^{th} single triangular element caused due to PC.

Semi analytic computation method (contd.)



42

- Considering a PC of M number of turns and N number of straight conductors in each turn, then at the center of the triangular element is calculated by (14).

$$\left(\overline{B}_{cent}\right)_i = \sum_{m=1}^M \sum_{n=1}^N \overline{B}_{cond} \quad (14)$$

- Here, M and N denotes number of turns in PC and number of straight current carrying conductor in a single turn of PC.
- The magnetic field due to a single straight current carrying conductor is calculated by Biot-Savart law (4).

$$\overline{B}_{cond} = \frac{\mu_o I}{4\pi R} (\sin \varphi_1 + \sin \varphi_2) \quad (15)$$

- The magnetic field due to whole PC at the center of the triangular element is given by (16).

$$\left(\overline{B}_{cent}\right)_i = \sum_{m=1}^M \sum_{n=1}^N \frac{\mu_o I}{4\pi R} (\sin \varphi_1 + \sin \varphi_2) \quad (16)$$

Semi analytic computation method (contd.)



43

- R is the perpendicular distance from the center of the triangular element (P) from the current carrying conductor. L is the length of the conductor, ϕ_1 and ϕ_2 are the geometrical angles and ϕ is the angle made by the differential element dl as shown in Fig. 20.

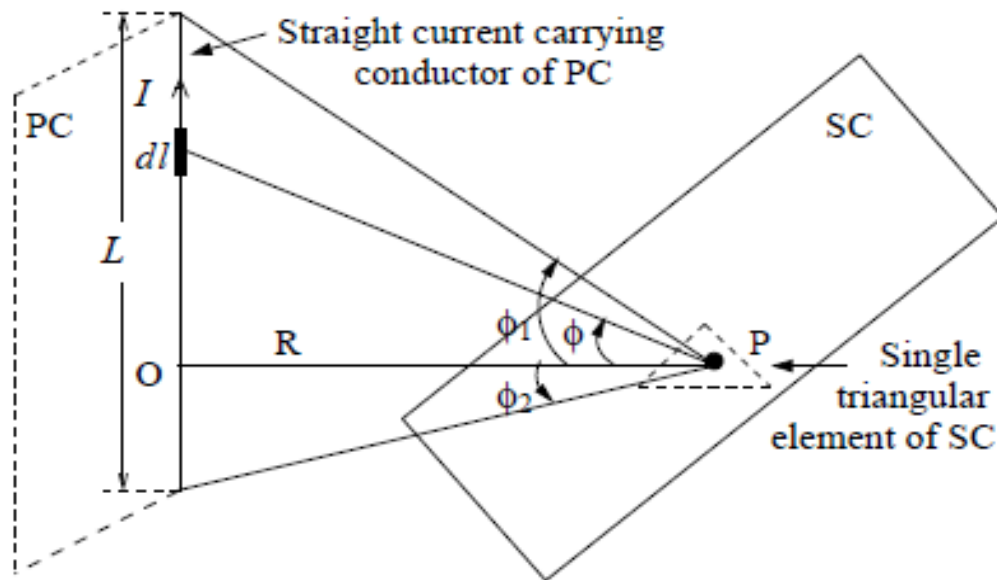


Fig. 20. Magnetic field due to a straight current carrying conductor.

Semi analytic computation method (contd.)



44

- The number of straight current carrying conductor N , used in (16) would vary for different coil geometry as given by (17). However, (16) is applicable only for straight current carrying conductor.

$$N = \left\{ \begin{array}{l} 4, \quad \text{rectangular coil} \\ 6, \quad \text{hexagonal coil} \\ 5, \quad \text{pentagonal coil} \end{array} \right\} \quad (17)$$

- To calculate the magnetic field due to circular and elliptical coils, these coil geometries are approximated with many small straight conductors and then expression (16) has been applied.
- A single turn of the circular coil approximated with multiple straight conductors such as x_0-x_1 , x_1-x_2 , x_2-x_3 , $x_{11}-x_0$.

Semi analytic computation method (contd.)



45

- Fig.21. shows the single turn of meshed hexagonal coil and approximation of single circular coil with multiple straight conductors

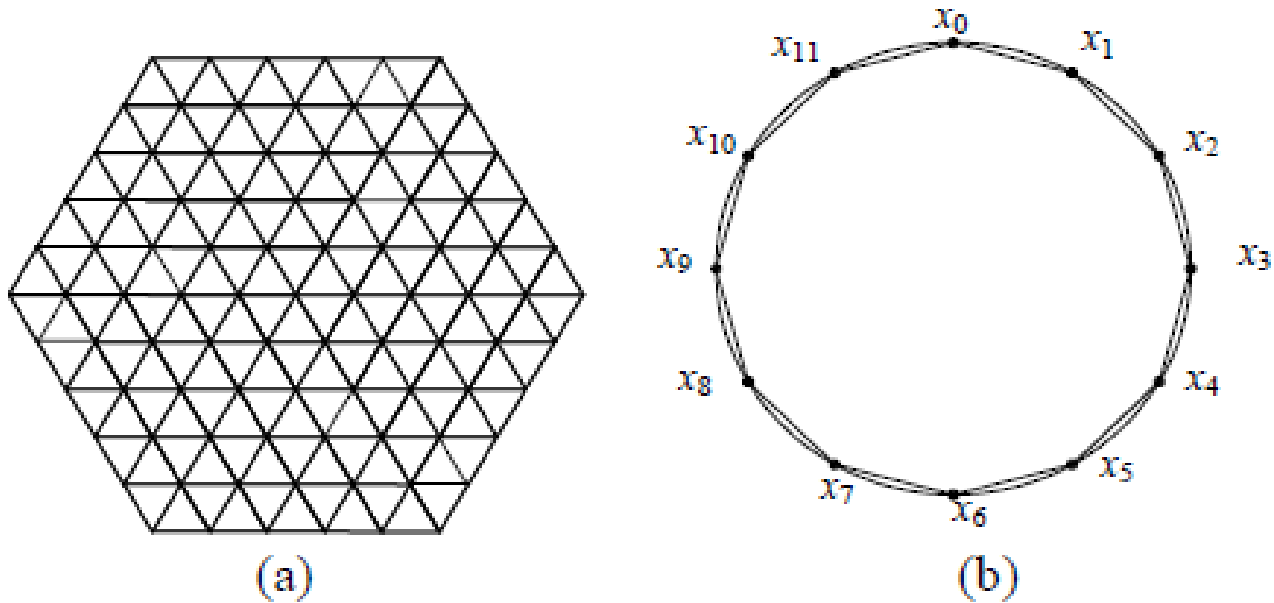


Fig. 21. a) Single turn of meshed hexagonal coil b) Approximation of circular primary coil with multiple straight current carrying conductor

Semi analytic computation method (contd.)



46

- The $(\vec{B}_{cent})_i$ obtained from (16) is used to calculate the flux crossing at the center of the triangular element.
- In similar manner, the flux crossing through all the triangular elements can be calculated and the total flux linked (φ_n) to a single turn of the SC is given by (18).

$$\varphi_n = \sum \varphi_1 + \varphi_2 + \dots + \varphi_Q \quad (18)$$

- By following the procedure explained from (13)-(18), the total flux linked to all the turns of the SC for a particular position is calculated, which is given by (19).

$$\lambda_{12} = \sum_{j=1}^p \sum_{n=1}^Q \varphi_n \quad (19)$$

- In this manner, MI is calculated for different misaligned cases of coil geometry using equations (13) - (19).

Automatic mesh generation

47

- Automatic mesh generating method is adapted for discretizing the coils of any geometry having curved surface and corners.
- In such cases, regular grid division may not be suitable, creating this type of mesh will result in fatal error.
- The program routine used in this work adopts an automatic mesh generation method [3], which considers every single turn of SC and discretize it into triangular element as shown in Fig. 21
- The selected coil turn of SC is first subdivided into quadrilateral block. The coordinates describing each block and the block topologies are specified as input data.
- Each block is represented by an eight-node quadratic isoparametric element with its local coordinate system

Automatic mesh generation (contd.)



48

- The local coordinate system (α, β) , is represented in terms of global coordinate system (x, y) as given by (20) and (21).

$$x(\alpha, \beta) = \sum_{i=1}^8 \psi_i(\alpha, \beta) x_i \quad (20)$$

$$y(\alpha, \beta) = \sum_{i=1}^8 \psi_i(\alpha, \beta) y_i \quad (21)$$

- Where, $\psi_i(\alpha, \beta)$ is a shape function associated with node i and (x_i, y_i) are the coordinates of node i defining the boundary of the quadrilateral block formed at the solution region.
- The obtained quadrilateral block is divided into quadrilateral elements.
- The size of the quadrilateral elements depends on the number of element subdivisions (N_α and N_β) in a and b directions and weighting factors $(W_\alpha)_i$ and $(W_\beta)_i$.
- The specification of weighting factors is required for allowing graded mesh within a block.

Automatic mesh generation (contd.)



49

- The initial a and b values are taken to be -1 , so that the natural coordinates are incremented according to (22) and (23).

$$\alpha_i = \alpha_i + \frac{2(W_\alpha)_i}{W_\alpha^T} \quad W_\alpha^T = \sum_{j=1}^{N_\alpha} (W_\alpha)_j \quad (22)$$

$$\beta_i = \beta_i + \frac{2(W_\beta)_i}{W_\beta^T} \quad W_\beta^T = \sum_{j=1}^{N_\beta} (W_\beta)_j \quad (23)$$

- Further, each quadrilateral element is divided into two triangular elements.
- This subdivision is done across the shortest diagonal of the quadrilateral element.
- The detailed explanation and an illustration of the evaluation procedure has been explained later.

Experimental Verification

50

- An image of different coils used for experimental verification is shown in Fig. 22. The values of L_p , L_s and C_f for different coil geometries are given in Table IV.

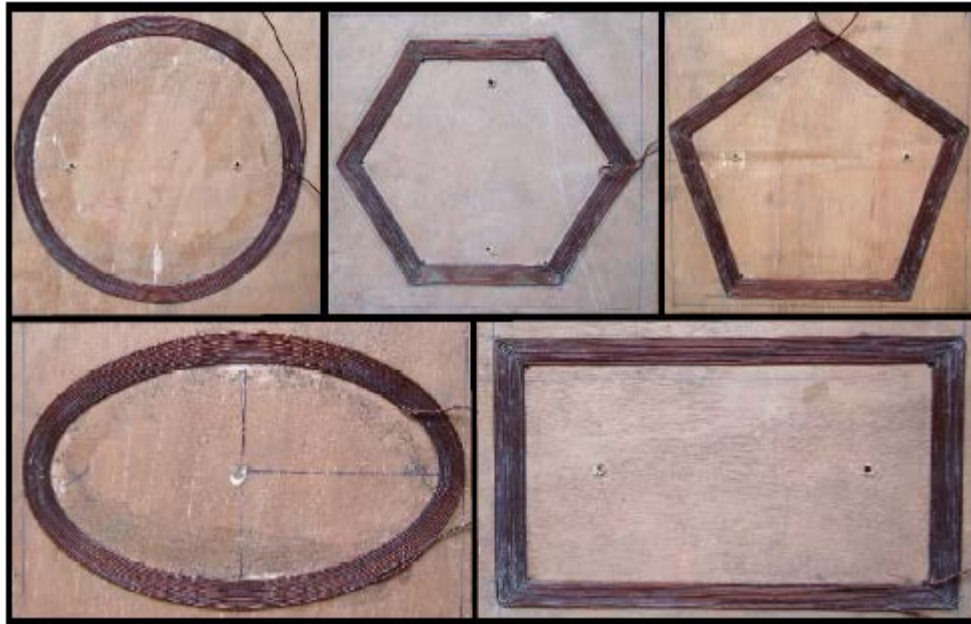


Fig. 22. Different coils used for experimental work.

Experimental Verification

- The values of L_p , L_s and C_f for different coil geometries are given in Table IV and dimensions of the coils is shown in Table V.

Type of coil geometry	L_p (μH)	L_s (μH)	C_f (μF)
Rectangle	34.366	34.55	2.27
Circle	36.222	36.84	2.16
Ellipse	26.744	26.77	2.92
Hexagon	30.472	28.92	2.56
Pentagon	32.178	32.17	2.43

Table IV
Specifications of inductance and capacitance

Parameter	Details
Thickness of copper strip	0.83mm
Diameter of copper	1.83mm
Width of the total turn	1.98cm
Copper track separation	0.008mm
Total length of the coil	5m
Number of turns in PC	10
Number of turns in SC	10

Table V
Dimensions of the coil

Results and Discussion

52

- Comparison of graphical plots between analytical method and experimental setup has been summarized. The results of five different coil geometries such as rectangular, circular, elliptical, hexagonal and pentagonal coils are discussed.
- Rectangular coil geometry** Fig. 23 and 24 shows the comparison of graphical plots of rectangular coil geometry for different misalignments

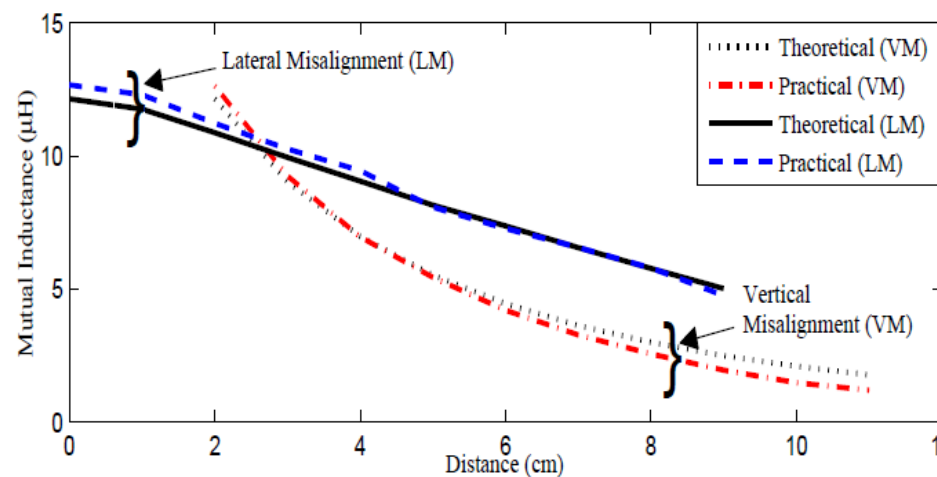


Fig.23. Rectangular coil - vertical and lateral misalignment

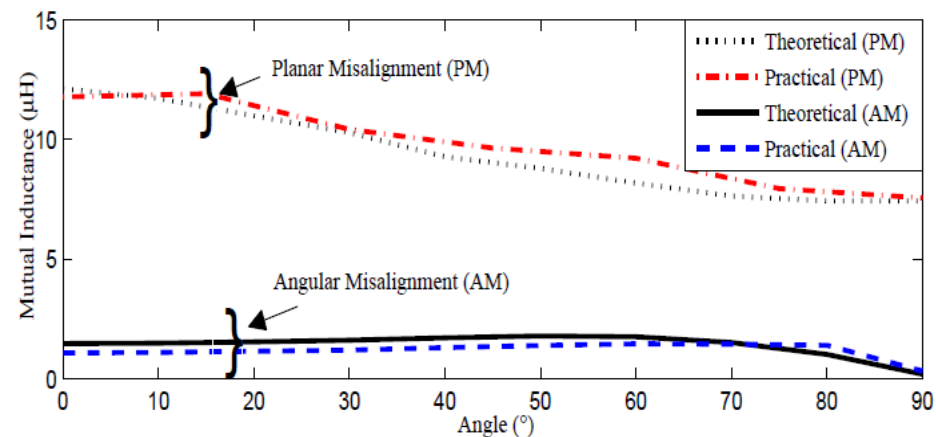


Fig. 24: Rectangular coil - planar and angular misalignment.

Results and Discussion (contd.)

53

Circular coil geometry

- Fig. 24 and 25 shows the comparison of graphical plots of circular coil geometry for different misalignments

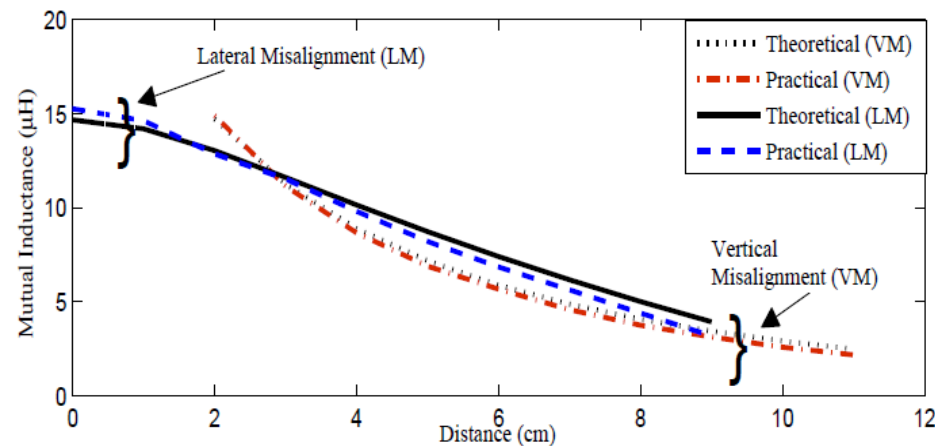


Fig.24. Circular coil- vertical and lateral misalignment

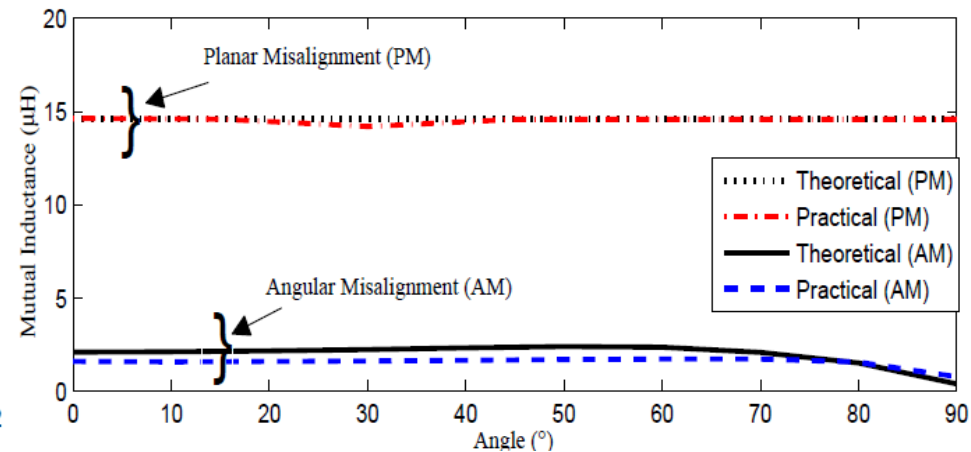


Fig. 25: Circular coil - planar and angular misalignment.

Results and Discussion (contd.)

54

Elliptical coil geometry

- Fig. 26 and 27 shows the comparison of graphical plots of elliptical coil geometry for different misalignments

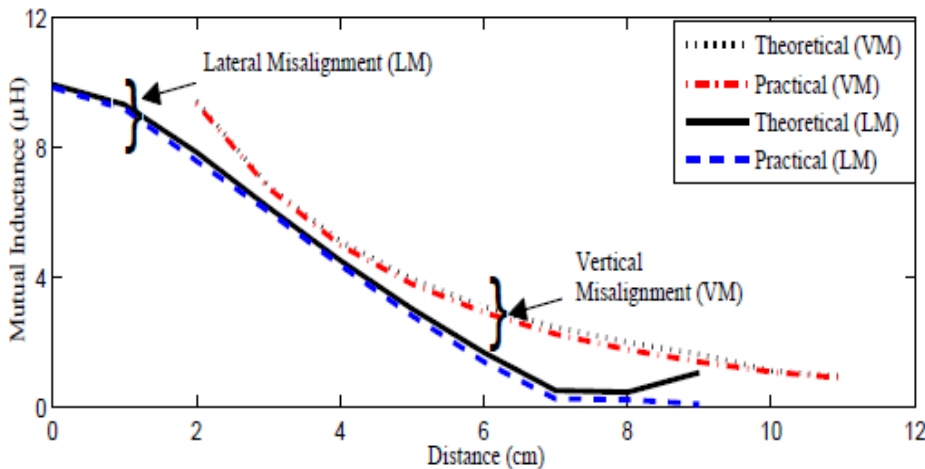


Fig.26. Elliptical coil- vertical and lateral misalignment

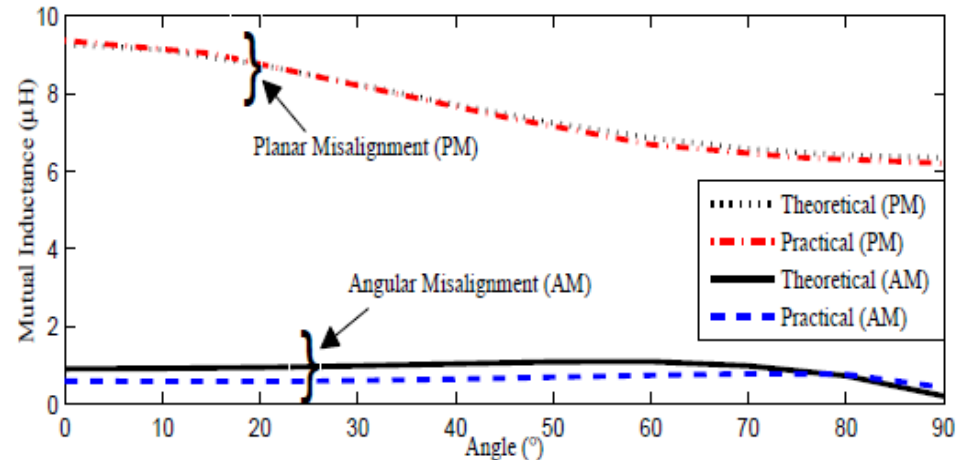


Fig. 27: Elliptical coil - planar and angular misalignment.

Results and Discussion (contd.)

55

Hexagonal coil geometry

- Fig. 28 and 29 shows the comparison of graphical plots of Hexagonal coil geometry for different misalignments

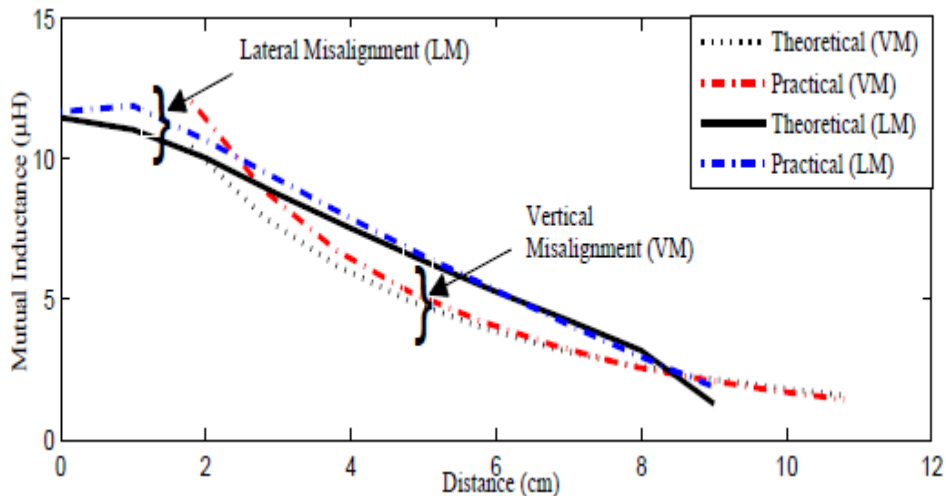


Fig.28. Hexagonal coil - vertical and lateral misalignment

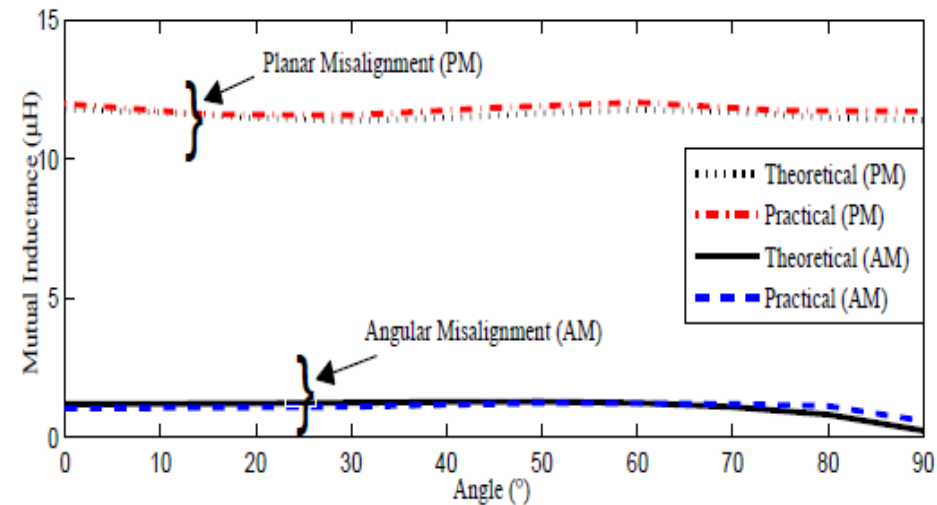


Fig. 29: Hexagonal coil - planar and angular misalignment.

Results and Discussion (contd.)

56

Pentagonal coil geometry

- Fig. 30 and 31 shows the comparison of graphical plots of pentagonal coil geometry for different misalignments

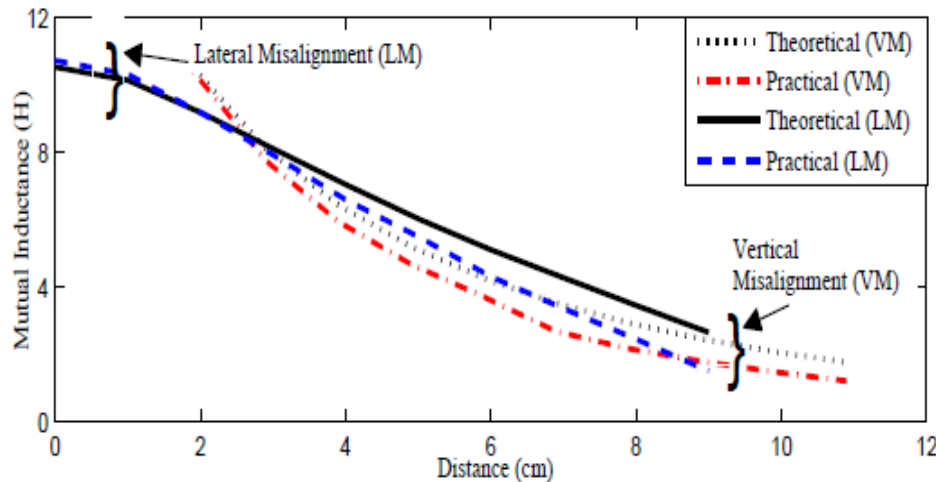


Fig.30. Pentagonal coil - vertical and lateral misalignment

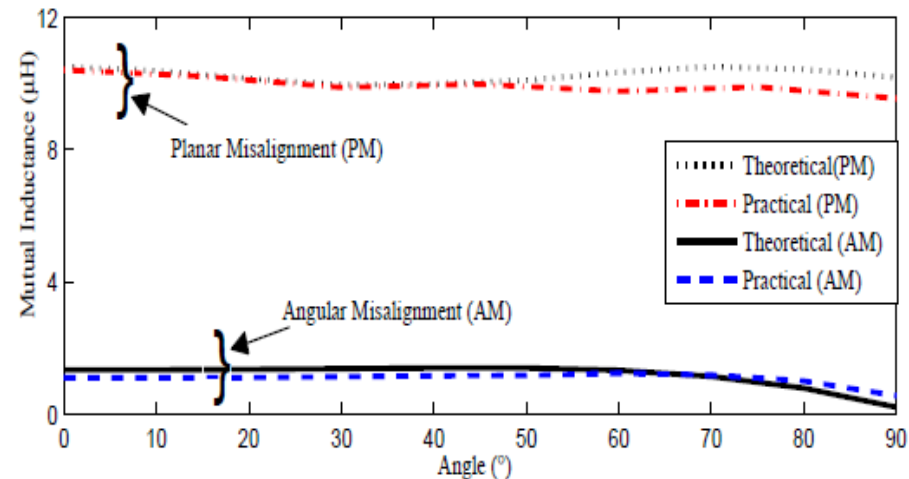


Fig. 31: Pentagonal coil - planar and angular misalignment.

Results and Discussion (contd.)

57

Comparison of change in MI

- Table VI shows percentage change in the values of MI for VM and LM between two values of initial and final position.
- In LM case rectangular coil shows the smallest change in MI value, when SC is moved from initial to final position and is most suited for lateral variation.
- It can be seen from the results that in case of PM, circular coil geometries shows greatest tolerance due to its regular geometry.
- The variation of AM of the coils has same pattern and the MI values are less as the experiment is performed at larger distance for all the coil geometries.

Table VI
Comparison of change in MI

	Rectangular	Circular	Elliptical	Hexagonal	Pentagonal
VM(%)	85.43	83.15	90.14	84.81	83.29
LM(%)	58.77	73.26	89.44	88.72	74.83

Results and Discussion (contd.)

□ Illustration of evaluation procedure

- To explain the computation procedure, circular coil geometry is chosen of radius 9cm.
- **Step I:** The circular solution region is defined using 21 nodes as shown in Fig. 32.
- The coordinates of the nodes (N) are obtained using the radius of the circle and are given in the Table VII.
- This circular solution region is divided into four quadrilateral isoparametric blocks each having eight nodes as shown in Table VIII.

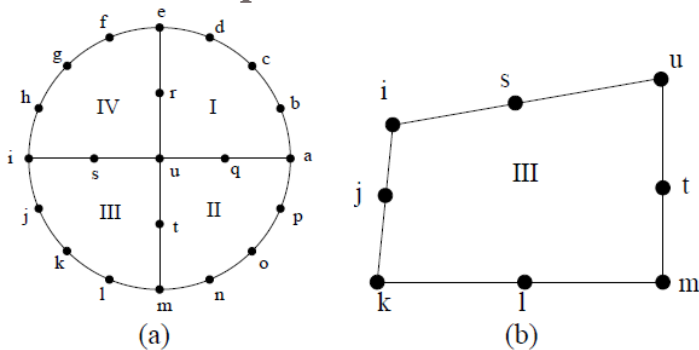


Fig.32. Circular solution region

(a) Subdivided solution region (b) single quadrilateral block describing coordinates at eight points.

N	x	y	N	x	y	N	x	y
a	9.00	0.00	h	-8.31	3.44	o	6.36	-6.36
b	8.31	3.44	i	-9.00	0.00	p	8.31	-3.44
c	6.36	6.36	j	-8.31	-3.44	q	4.50	0.00
d	3.44	8.31	k	-6.36	-6.36	r	0.00	4.50
e	0.00	9.00	l	-3.44	-8.31	s	-4.50	0.00
f	-3.44	8.31	m	0.00	-9.00	t	0.00	-4.50
g	-6.36	6.36	n	3.44	-8.31	u	0.00	0.00

Table VII: Coordinates of the node

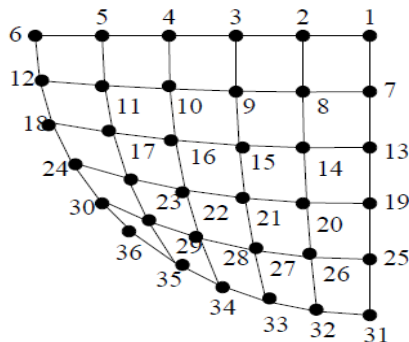
Block	Nodes
I	a-b-c-d-e-r-u-q-a
II	a-p-o-n-m-t-u-q-a
III	i-j-k-l-m-t-u-s-i
IV	e-f-g-h-i-s-u-r-e

Table VIII: Nodes of the quadrilateral block

Results and Discussion (contd.)

□ Illustration of evaluation procedure (contd.,)

- Local coordinate (LC(α , β)) system corresponding to the global coordinates (GC(x, y)) for each node is defined and is given in Table IX.
- **Step 2:** This step involves subdivision of the quadrilateral block into elements, considering N_α and N_β to be 5. For convenience, $(W_\alpha)_i$ and $(W_\beta)_i$ are taken to be 1.
- Fig. 33 shows the subdivided quadrilateral elements, where 1 to 36 represents the nodes of the quadrilateral elements.
- In which, the results of 10 node obtained from the program for GC and LC is shown in Table X.



N	GC		LC		N	GC		LC	
	x	y	α	β		x	y	α	β
k	-6.36	-6.36	-1	-1	u	0.00	0.00	1	1
j	-8.31	-3.44	-1	0	t	0.00	-4.50	1	0
i	-9.00	0.00	-1	1	m	0.00	-9.00	1	-1
s	-4.50	0.00	0	1	l	-3.44	-8.31	0	-1

N	GC (cm)		LC		N	GC (cm)		LC	
	x	y	α	β		x	y	α	β
1	0.00	0.00	-1.0	-1.0	6	-9.00	-0.01	1.0	-1.0
2	-1.80	0.00	-0.6	-1.0	7	0.00	-1.80	-1.0	-0.6
3	-3.60	0.00	-0.2	-1.0	8	-1.81	-1.81	-0.6	-0.6
4	-5.40	0.00	0.2	-1.0	9	-3.60	-1.78	-0.2	-0.6
5	-7.20	0.00	0.6	-1.0	10	-5.37	-1.71	0.2	-0.6

Fig. 33: Meshed quadrilateral block

Table IX: Global and local coordinate

Table X: GC and LC for nodes of quadrilateral element

Results and Discussion (contd.)

Illustration of evaluation procedure (contd.)

- Fig. 34 shows the division of each quadrilateral element into 50 triangular elements.
- Table VIII has shown the node numbers of only 10 triangular element as an example.
- Step 3: A single triangular element having node numbers 1, 2 and 8 (element number 1 in Fig. 33) is considered as shown in Fig.

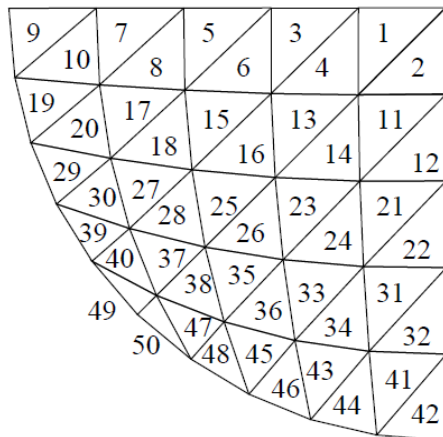


Fig. 33: Quadrilateral element

Element	Node number			Element	Node number		
	N_1	N_2	N_3		N_1	N_2	N_3
1	1	2	8	6	3	10	9
2	1	8	7	7	4	5	11
3	2	3	9	8	4	11	10
4	2	9	8	9	5	6	12
5	3	4	10	10	5	12	11

Table XI: Node numbers for 10 triangular elements

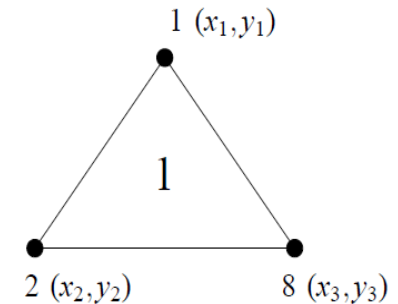


Fig. 34: Single triangular element

Results and Discussion (contd.)

61

Illustration of evaluation procedure (contd.,)

- The coordinates of the chosen triangular element is taken from Table VII are (x_1, y_1, z_1) is $(0, 0, 0.02)$, (x_2, y_2, z_2) is $(-0.018, -2.3 \times 10^{-5}, 0.02)$ and (x_3, y_3, z_3) is $(-0.01806, -0.01812, 0.02)$.
- As the secondary coil is placed at a height of 2cm, the z coordinate is taken as 0.02m.
- Using this coordinates, the \square_{A_1} , A_1 and $(\vec{B}_{cent})_1$ are calculated using (14).
- The values of \square_{A_1} , A_1 and $(\vec{B}_{cent})_1$ are given below.

$$\varphi_1 = 1.13 \times 10^{-7} \text{ wb} \quad \square_{A_1} = 0\hat{x} + 0\hat{y} + 1\hat{z} \quad A_1 = 1.6308 \times 10^{-4} \text{ m}^2$$

- On substituting these values, the flux φ_1 crossing through the triangular element is calculated by (13) as given below:

$$(\vec{B}_{cent})_1 = -3.33 \times 10^{-5} \hat{x} - 1.69 \times 10^{-5} \hat{y} + 6.9082 \times 10^{-4} \hat{z}, \text{ wb / m}^2$$

Results and Discussion (contd.)

62

□ Illustration of evaluation procedure (contd.)

- In similar way, the flux crossing through all the surfaces of the triangular elements are calculated and added together to get the flux crossing through one turn of the secondary coil by (18).
- Table IX shows the flux linkage (φ_n) value of all the turns of circular secondary coil. 4.08×10^{-5}
- In order to obtain the total flux linked to the secondary coil (λ_{12}), the above said procedure is repeated for all the turns of the secondary coil using (19).
- λ_{12} value is the summation of (φ_n) which is given by
- By substituting this value MI value is calculated as 4.08×10^{-6} , using the formula given in (1).

Results and Discussion (contd.)

Illustration of evaluation procedure (contd.)

Turn	Flux ($10^{-6}Wb$)	Turn	Flux ($10^{-6}Wb$)
Turn 1	4.26	Turn 6	4.09
Turn 2	4.24	Turn 7	4.03
Turn 3	4.22	Turn 8	3.96
Turn 4	4.18	Turn 9	3.89
Turn 5	4.14	Turn 10	3.80
Total Flux (λ_{12})	$4.08 \times 10^{-5}Wb$		
MI	$4.08 \times 10^{-6}H$		

Table XII: Flux linkage Calculation

Mutual inductance for coils of different geometries (Contd.)



64

- A 2 kw hardware prototype of contactless charging system is planned to develop in our lab to check G2V and V2G process, which is already on the process on the process of development.
- H-Bridge converter and resonant converters will be build in our lab shortly with different types of controllers such as spartan 3E FPGA board, kiel Microprocessor kit, sliding mode , adaptive sliding mode controller etc to check its robustness of controlling contactless coils.
- Effect of compensation topologies in contactless system with respect to variations in frequency, load resistance and efficiency is going to be checked very shortly

References

- [1] Joy E. R, Dalal. A and Kumar P., “The Accurate Computation of Mutual Inductance of Two Air Core Square Coils with Lateral and Angular Misalignments in a Flat Planar Surface”, *IEEE Transactions on Magnetics*, vol. 0, pp. 1, 2013.
- [2] Dalal. A, Joy E. R and Kumar P., “The Accurate Computation of Mutual Inductance of Two Air Core Square Coils with Lateral and Angular Misalignments in a Flat Planar Surface”, submitted on *IEEE Transactions on Industrial Electronics*.
- [3] M.N.O. Sadiku, “*Numerical techniques in elctromagnetics*”, 2nd, Ed. CRC Press, 2001.